III. RADIO ASTRONOMY*

Academic and Research Staff

Prof A. H. Barrett
Prof. B. F. Burke
Prof. R. M. Price
Prof. D. H. Staelin
Dr. S. H. Zisk
J. W. Barrett
O. H. Gonzalez
D. C. Papa
C. A. Zapata

Graduate Students

R. M. Blotky
M. S. Ewing
N. E. Gaut
W. W. Gebhart
L. P. A. Henckels
H. F. Hinteregger
Sara E. Law
J. M. Moran, Jr.
P. C. Myers
G. D. Papadopoulos
E. C. Reifenstein III
P. W. Rosenkranz
L. W. Schaper, Jr.
P. R. Schwartz
J. W. Waters
T. T. Wilheit, Jr.
T. L. Wilson
W. J. Wilson

A. LONG BASELINE INTERFEROMETER EXPERIMENTS

Another very long baseline interferometer experiment was successfully carried out between January 28 and 31, 1968. Its purpose was to extend the study of the structure of OH radio sources. The interferometer had 4 elements consisting of the radio telescopes at the Haystack Microwave Research Facility of Lincoln Laboratory, M.I.T., Westford, Mass., National Radio Astronomy Observatory, Green Bank, West Virginia, University of California Observatory, Hat Creek, California, and Chalmers University Observatory, Onsala, Sweden. At each site atomic frequency standards were used to control the local oscillators and thereby make the system phase coherent. The signals received at each site were sampled and recorded on magnetic tape, the sampling being controlled by the frequency standard. The time synchronization at the stations in Westford, Green Bank, and Sweden was achieved by having all stations monitor the Loran C transmission of the North Atlantic chain. At Hat Creek the clock was synchronized to the Hewlett-Packard traveling clock.

Figure III-1 shows a complex visibility spectrum on W3 obtained by crosscorrelating the data on tapes taken at Haystack and Onsala, Sweden. The processing time for this 80-sec integration period was 160 minutes on a CDC-3300 computer. The bulk of this time was taken up with computing the crosscorrelation function, which required performing 4×10^9 1-bit multiplications. The single antenna spectrum has spectral features at -41.7, -43.7 and -45.1 km/sec. The feature at -45.1 is the strongest but shows low visibility, which implies that it is resolved on this baseline. The difference in fringe phase among the features indicates their spatial

*This work was supported principally by the National Aeronautics and Space Administration (Grant NsG-419 and Contract NSR-22-009-120); and in part by the Joint Services Electronics Programs (U.S. Army, U.S. Navy, and U.S. Air Force, under Contract DA 28-043-AMC-02536(E), the U.S. Navy (Office of Naval Research) under Contract N00014-67-A-0204-0009, and the National Science Foundation (Grant GP-7046).

separation. The phase shift across the -41.7 km/sec feature is probably caused by a change in position of the feature with velocity. The fringe amplitude of the -43.7 km/sec was computed on each of the 6 baselines by crosscorrelating all possible pairs among the 4 elements. The results (see Fig. III-2) show a systematic decrease in fringe amplitude with increased baseline, which indicates that the feature

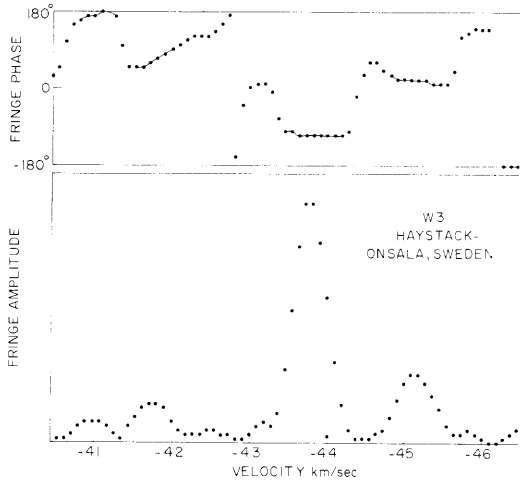

Fig. III-1. Visibility spectrum on W3 in right circular polarization. Interferometer elements were at Haystack and Onsala, Sweden, giving a baseline of 5600 km. The spatial resolution is 0.007 second of arc, and the velocity resolution is 0.4 km/sec.

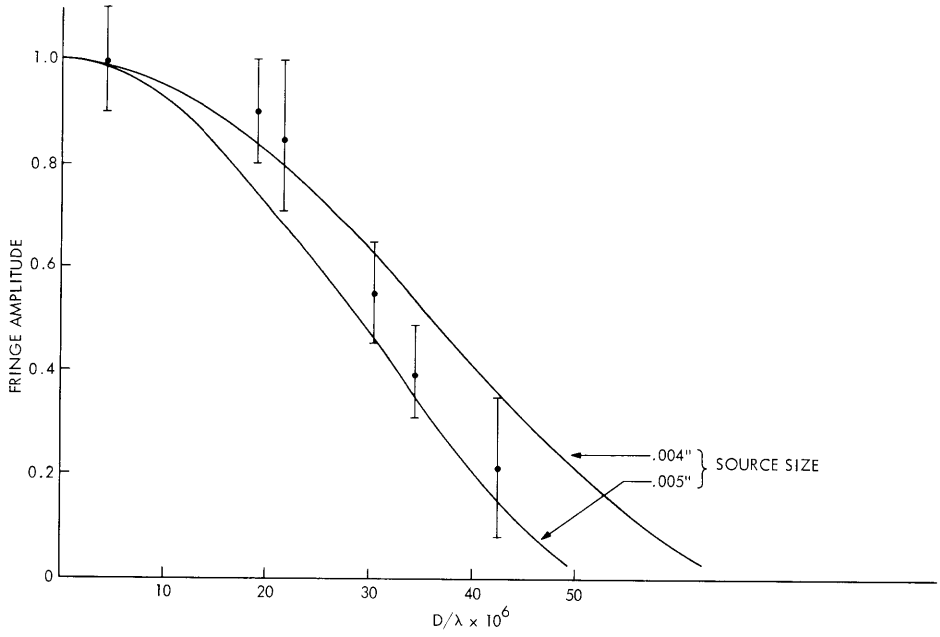

Fig. III-2. Fringe amplitude vs projected baseline length for the -43.7 km/sec feature in W3. The 6 points were obtained by crosscorrelating the 4 data tapes recorded simultaneously with all possible pairs. The baselines in order of length are Haystack-NRAO, Berkeley-NRAO, Berkeley-Haystack, Haystack-Onsala, NRAO-Onsala, and Berkeley-Onsala.

is being resolved. Its diameter is 0.0045 second of arc if a uniform disk model is assumed or approximately 0.0025 second of arc between half-power points if a Gaussian distribution is assumed. The diameter 0.0045 second of arc corresponds to a linear distance of approximately 7 A.U. There does not seem to be any great change in fringe amplitude with baseline orientation, which means that this feature is roughly circular in shape.

The operation of a multielement interferometer involved no additional development of the equipment that was used in the experiments between 2 stations last summer. The experiment is important, in that it showed that a multielement system can be operated successfully without serious coordination problems, thereby making more data available per tape recording, because of the increased number of possible correlations. Furthermore, with 3 or more antenna simultaneously observing, some severe instrumental effects can be overcome. For example, the effects of phase and frequency uncertainty in the atomic standards can be eliminated to achieve accurate position measurements of the

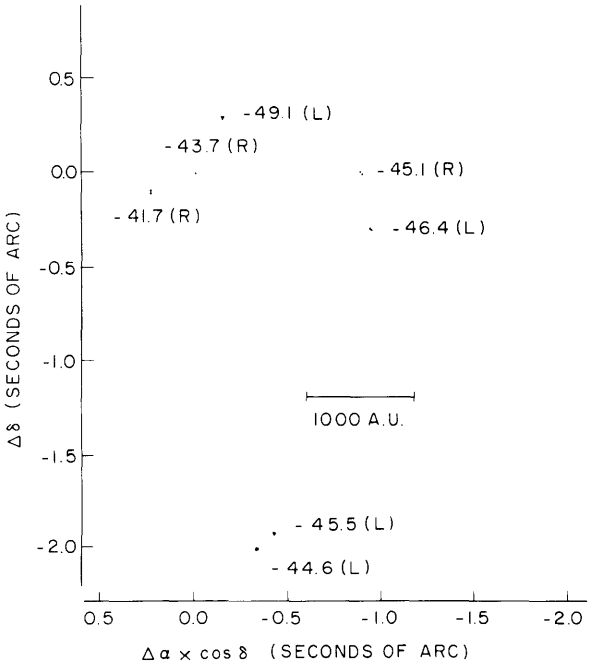

Fig. III-3. Map of W3 OH source. The position separations among the features were determined from the relative fringe-rate information. The absolute position of the map is uncertain to ±5 second of arc.

baselines and source position of the order of 0.001 second of arc, provided the atmospheric refraction problems can be solved.

We have improved the map of the W3 region that was presented in Quarterly Progress Report No. 88 (page 29). The new map, shown in Fig. III-3, shows all seven of the major features in the W3 spectrum at the 1665-MHz transition. The features at -49.1(L), -45.5(L) and -46.4(L) km/sec have a complex structure of the order of

0.02 second of arc. The -45.1(R) and -41.7(R) km/sec features are double, with separations of the order of 0.02 second of arc. The feature at -43.7(R) km/sec is 0.0045 second of arc in size, and approximately circular in shape. The separations among the features were determined by analyzing the difference in fringe rate of the features as a function of local hour angle. The technique is free of ambiguity problems and instrumental effects, although its sensitivity is rather low. The errors in the positions are typically ±0.3 second of arc.

J. M. Moran, A. H. Barrett, B. F. Burke

B. RADIO INTERFEROMETER

A front-end prototype of the 1.75-cm radio interferometer has been constructed, and one of the dishes has been used in rudimentary observations of the sun.

Slew drives are now being installed in the antenna mounts.

The digital interface and phase-lock mechanism are in the final stages of testing.

The analog multipliers, as well as the calibration and delay compensation circuits, are currently under construction.

G. Papadopoulos, M. S. Ewing, D. C. Papa, B. F. Burke

C. MIT-NRAO RECOMBINATION LINE SURVEY

The MIT-NRAO recombination line survey observations are now complete for the Northern Hemisphere. We have observed all sources in the NRAO 11-cm survey[1] down to an antenna temperature of 1°K at 6 cm on the 140-ft radio telescope. There are 120 sources in all, and recombination lines were found in 75 of these. These data are now being prepared for publication.

Our results indicate that except for the Sagittarius sources there are no H II regions inside the 4-kpc arm. Observations by Costain[2] and Altenhoff[3] indicate that those sources that have no recombination line are nonthermal. Observation of Helium in M17, Orion, and W49 indicates a Helium/Hydrogen ratio of approximately 9% by number.

T. L. Wilson, E. C. Reifenstein, B. F. Burke

References

1. W. A. Altenhoff and P. G. Mezger, in preparation.
2. C. Costain, Private communication, 1968.
3. W. A. Altenhoff, Private communication, 1968.

D. K-BAND OBSERVATIONS OF STRATOSPHERIC WATER VAPOR

The microwave spectrum of the terrestrial atmosphere at frequencies within 100 MHz of the 22.235-GHz water-vapor resonance is very sensitive to the abundance of water vapor at high altitudes. Direct rocket and balloon measurements of the water-vapor content are usually limited to altitudes below 30 km, so microwave measurements can be valuable in extending the water-vapor profile to higher altitudes.

Measurements to detect high-altitude water vapor were made using a 16-channel radiometer[1] during the period August 1967-January 1968. The radiometer was a superheterodyne system with IF passband 20-84 MHz without image rejection. Each channel was 4 MHz wide, and successive channels overlapped at the half-power points. The theoretical half-width of the water-vapor line is 42 MHz at 30 km and 3 MHz at 50 km, so the measurements would be most sensitive to water vapor between these altitudes.

The measurements were made using 2 microwave horns, each of 15° beamwidth. Reflectors were positioned in front of the horns so that one horn received radiation from the sky at 10° from the zenith, and the other horn received radiation at 78° from the zenith. An absorber at ambient temperature was placed partially in the beam of the 10° horn in order to approximately equalize the temperature received by the two horns. The data runs consisted in (i) a 4-minute calibration, (ii) 8 integrations of 4 minutes each, alternating between the two horns, and (iii) another 4-minute calibration. The difference in temperature between the two horns was computed and normalized to have a zero mean over the 16 channels. The difference spectrum would be expected to show an emission feature, since the path length through the atmosphere is greater for the 78° horn.

To minimize the effects of interference in the experimental spectra, data points were discarded if they showed large rms deviations during a run or if they had values deviating more than 0.5°K from the mean of the 16 channels. The spectra were smoothed by computing a weighted average (1-2-2-1) over each set of 4 channels. Figure III-4 shows 4 experimental and theoretical spectra labeled by date. If the errors are correlated from channel to channel, the larger error bracket is applicable, but if the errors are uncorrelated as they should be, then the smaller error bracket applies. These error brackets represent only the rms receiver noise. In order to detect spurious channel-dependent spectral features, each data set was made with a difference local-oscillator frequency, as noted in Fig. III-4. No such effects are evident.

The theoretical spectra were computed using typical summer temperature and pressure profiles. The theoretical water-vapor profile was based on measurements of Sissenwine et al.[2] made at Chico, California, for altitudes below 30 km. These measurements were extrapolated to the 30-60 km region by assuming a constant

mixing ratio of 1.4×10^{-5} for this region. The 4 theoretical spectra were computed for the same model atmosphere. They appear different because each was folded about the

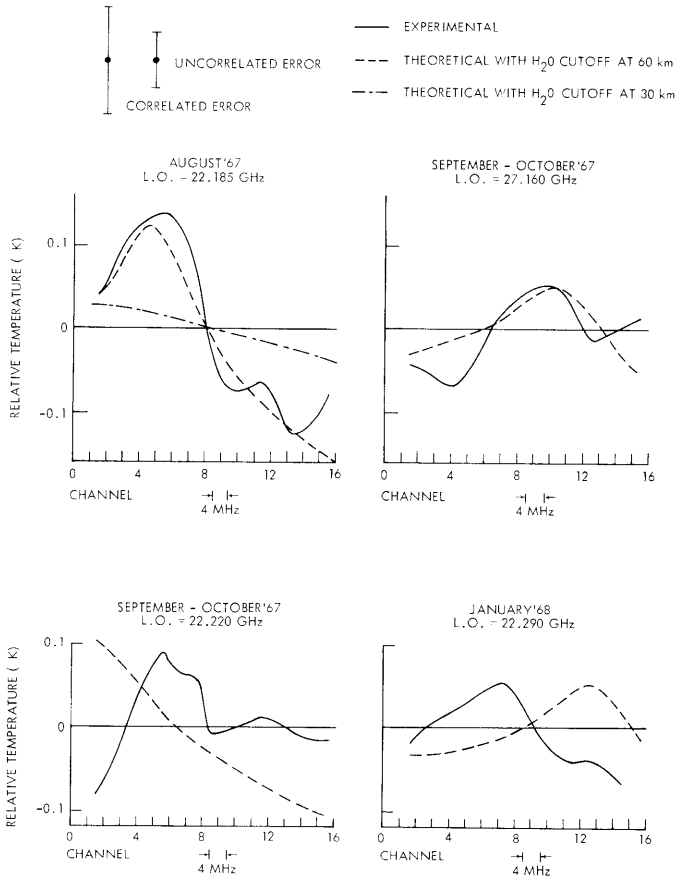

Fig. III-4. Four experimental and theoretical spectra.

appropriate local-oscillator frequency to simulate the effect of double sidebands. Figure III-4 shows good agreement between theoretical and experimental spectra for the August 1967 data. The observed spectral feature deviates from a flat spectrum by more than 2 standard deviations. The theoretical spectrum for no water vapor above 30 km is shown for comparison with the August data.

The measurements during the September-January period show no features at the expected frequency larger than 1 standard deviation, and thus one can only conclude that the high-altitude water vapor did not increase significantly during the fall and winter.

These preliminary data support the data of Sissenwine et al.,[2] but further measurements to confirm these results will be very helpful.

Sara E. Law, R. Neal, D. H. Staelin

References

1. D. H. Staelin, R. M. Weigand, and J. M. Waters, "20-channel Microwave Radiometer," Quarterly Progress Report No. 86, Research Laboratory of Electronics, M.I.T., July 15, 1967, pp. 25-26.
2. N. Sissenwine, D. D. Grantham, and H. A. Salmels, "Mid-Latitude Stratospheric Humidity Regime to 30 km," Interim Notes on Atmospheric Properties No. 73, Presented at AFCRL Scientific Balloon Symposium, Portsmouth, New Hampshire, September 14, 1966.

E. STATISTICAL INVERSION OF RADIOMETRIC DATA

The statistical data inversion technique presented here is an extension of that described in previous reports.[1,2] From a set of measurable quantities, represented by a data vector $\underline{d}$, one wishes to infer certain parameters represented by a parameter vector $\underline{p}$. Let $\underline{p}^*$ be the inferred value of $\underline{p}$. We represent $\underline{p}^*$ as a combination of some basis functions ϕ_i of the raw data:

$$\underline{p}^* = \underline{\underline{D}} \cdot \underline{\phi}(\underline{d}),$$

where $\underline{\underline{D}}$ is a matrix to be determined. No restrictions are placed on the functions $\phi_i(\underline{d})$. They may be linear or nonlinear, and need not be orthogonal or complete. They are chosen from one's knowledge of the physical relation between $\underline{p}$ and $\underline{d}$. $\underline{\underline{D}}$ is found from the statistics of $\underline{p}$ and $\underline{d}$ by minimizing the expected mean-square error in $\underline{p}^*$

$$\underline{\underline{D}} = \underline{\underline{C}}(\underline{p}, \underline{\phi}) \cdot \underline{\underline{C}}^{-1}(\underline{\phi}, \underline{\phi}), \tag{1}$$

where

$$C_{ij}(\underline{x}, \underline{y}) = \langle x_i y_j \rangle$$

is the correlation matrix. In general, $\underline{d} = \underline{d}^\circ + \underline{n}$, where $\underline{d}^\circ$ represents noiseless data, and $\underline{n}$ is additive noise. Expanding $\underline{\phi}$ in a Taylor series yields for the correlation matrices

$$C_{ij}(\underline{p}, \underline{\phi}) = C_{ij}[\underline{p}, \phi/\underline{d}^\circ)] + \sum_{k=1}^{\infty} \frac{1}{k!} \left\langle p_i (\underline{n} \cdot \nabla_d)^k \phi_j(\underline{d}) \right\rangle \Big|_{d=d^\circ}$$

$$C_{ij}(\phi, \phi) = C_{ij}[\underline{\phi}(\underline{d}^\circ), \underline{\phi}(\underline{d}^\circ)] + \sum_{k=1}^{\infty} \frac{1}{k!} \left\langle (\underline{n} \cdot \nabla_d)^k \phi_i(\underline{d})\, \phi_j(d) \right\rangle \Big|_{d=d^\circ},$$

where ∇_d is the del operator in $\underline{d}$-space.

A problem arises when $\underline{\underline{C}}(\underline{\phi}, \underline{\phi})$ is singular, since then its inverse does not exist and Eq. 1 is meaningless. When this occurs one chooses a new set of basis functions $\underline{\phi}'$ for

which $\underline{\underline{C}}(\underline{\phi}', \underline{\phi}')$ is diagonal. Since $\underline{\underline{C}}$ is Hermitian, it can be shown that $\underline{\phi}'$ is related to $\underline{\phi}$ by

$$\underline{\phi}' = \underline{\underline{R}}^t \underline{\phi},$$

where $\underline{\underline{R}}^t$ is the transpose of the matrix formed from the normalized (column) eigenvectors of $\underline{\underline{C}}(\underline{\phi}, \underline{\phi})$. The singularity of $\underline{\underline{C}}$ is caused by those functions ϕ_j' for which $C_{jj}(\underline{\phi}', \underline{\phi}')$ is zero, or is below the computational noise level. These ϕ_j' are discarded, and the remaining ϕ_i' are used in the following expression for $\underline{p}^*$:

$$\underline{p}^* = [\underline{\underline{C}}(\underline{p}, \underline{\phi}') \cdot \underline{\underline{C}}^{-1}(\underline{\phi}', \underline{\phi}')] \cdot \underline{\phi}'(\underline{d}). \tag{2}$$

Equation 2 gives the value of $\underline{p}^*$ which minimizes its expected mean-square error for given a priori statistics and basis functions $\underline{\phi}(\underline{d})$. This inversion technique is very general and can be applied to a variety of problems. It requires only statistical knowledge of the parameters and data or a means of generating these statistics. The physical relationship between parameter and data is not necessarily required.

The inversion technique described above has been used in numerical experiments for determining tropospheric temperature and water-vapor profiles by microwave radiometry. Statistical information was computed from radiosonde records obtained from the U. S. Weather Bureau.

The results of 100 inversions for total water vapor in various layers of the atmosphere are shown in Table III-1. The data vector for these inversions consists of computed brightness temperatures as would be observed in emission against a cold sky, by an ideal radiometer at the surface looking toward the zenith. The frequencies were 20.0 and 22.0 GHz, which are near the 22.235-GHz resonance of water vapor. Inversions were performed from noiseless data and from data to which 1°K rms noise had been added. Table III-1A gives results for a linear inversion in which the data basis function vector $\underline{\phi}(\underline{d})$ equals the data vector $\underline{d}$. Table III-1B shows the improvement obtained by augmenting the linear basis function vector with the nonlinear function $\phi_3(\underline{d}) = d_1 d_2$. Also indicated are the mean and the standard deviation σ of the parameter. The standard deviation of the parameter tells how accurately its value can be determined before making a measurement. Comparison of this with the standard deviation in the inversion errors gives the value of the measurement.

Inversions for tropospheric water vapor were also performed from data simulating that which would be collected by a radiometer looking down at nadir from an orbiting satellite. The results are approximately the same as those given in Table III-1 when the satellite is over a calm ocean. When the satellite is over land, little information about tropospheric water vapor is obtained.

Figure III-5 shows the results of 100 linear inversions for tropospheric temperature profiles from data simulating that collected by an orbiting radiometer. The data

Table III-1. Inversion results for water vapor.
(Based on 100 radiosonde records. Kwajalein and Tucson, Arizona.)

A. Linear Inversion

Parameter	Parameter Statistics		Inversion Errors		Receiver Sensitivity
	mean	σ	mean	σ	°K
$\int_{4\,km}^{9.5\,km} \rho_{H_2O}\, dh \ \frac{gm}{cm^2}$	0.42	0.38	.04	.17	0
			.02	.18	1
$\int_{2\,km}^{4\,km} \rho_{H_2O}\, dh \ \frac{gm}{cm^2}$	0.83	0.55	.01	.13	0
			.01	.13	1
$\int_{0}^{2\,km} \rho_{H_2O}\, dh \ \frac{gm}{cm^2}$	1.94	1.21	-.02	.19	0
			.01	.21	1
$\int_{0}^{9.5\,km} \rho_{H_2O}\, dh \ \frac{gm}{cm^2}$	3.19	2.03	.03	.07	0
			.04	.09	1

B. Nonlinear Inversion

Parameter	Parameter Statistics		Inversion Errors		Receiver Sensitivity
	mean	σ	mean	σ	°K
$\int_{4\,km}^{9.5\,km} \rho_{H_2O}\, dh \ \frac{gm}{cm^2}$	0.42	0.38	-.01	.11	0
			.00	.16	1
$\int_{2\,km}^{4\,km} \rho_{H_2O}\, dh \ \frac{gm}{cm^2}$	0.83	0.55	.00	.13	0
			.00	.13	1
$\int_{0}^{2\,km} \rho_{H_2O}\, dh \ \frac{gm}{cm^2}$	1.94	1.21	-.01	.14	0
			.01	.20	1
$\int_{0}^{9.5\,km} \rho_{H_2O}\, dh \ \frac{gm}{cm^2}$	3.19	2.03	.00	.02	0
			.00	.08	1

comprised calculated brightness temperatures at three frequencies in the oxygen absorption band around 60 GHz. The algebraic mean and the standard deviation σ of

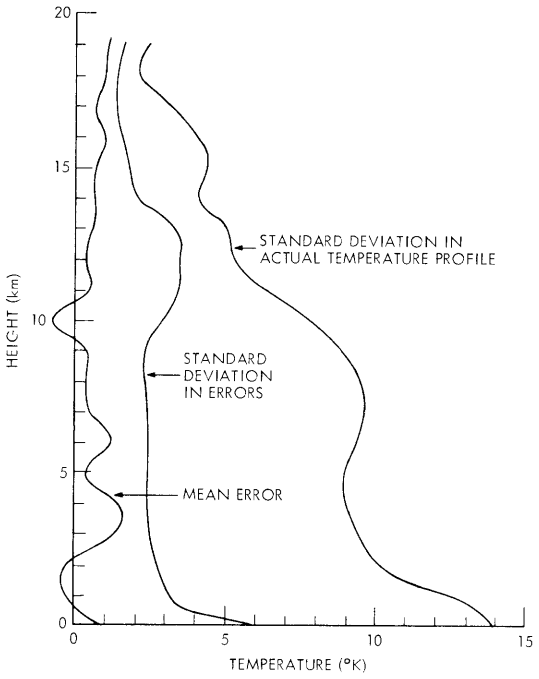

Fig. III-5. Errors in inversions for temperature profile based on statistics from 100 radiosonde records and 100 inversions. Data are calculated brightness temperatures at frequencies 53.60, 60.82, and 64.47 GHz. When looking down at nadir from a 20-km surface, the emissivity is 1.0. The calculations shown here are for noise-free data.

the 100 inversion errors are plotted as a function of altitude. For comparison, the standard deviation in the actual temperature profile is shown. Preliminary investigations indicate that the results shown in Fig. III-5 are independent of the surface below the satellite and the statistics used for calculations. From these results, it appears that the tropospheric temperature profile can be determined within approximately 3°K by passive microwave techniques.

The results presented in this report should be considered preliminary for two reasons: the choice of nonlinear basis functions $\underline{\phi}(\underline{d})$ has not been fully explored or optimized, and some of the matrices that had to be inverted were slightly singular and results have not yet been obtained by using the method described here for getting around the problem of inverting singular matrices. This work will continue.

J. W. Waters, D. H. Staelin

References

1. D. H. Staelin, "Interpretation of Spectral Data," Quarterly Progress Report No. 85, Research Laboratory of Electronics, M. I. T., April 15, 1967, pp. 15-16.
2. N. E. Gaut, A. H. Barrett, and D. H. Staelin, "Results Obtained from the Inversion of Simulated Atmospheric Water-Vapor Spectra," Quarterly Progress Report No. 85, Research Laboratory of Electronics, M. I. T., April 15, 1967, pp. 16-19.